Iranian Journal of Geophysics, Vol 18 No 6, 2025, Page 95 – 110 (Research Article)
DOI: 10.30499/ijg.2024.431652.1558

A fast implementation of stochastic 1D elastic seismic full-waveform inversion

Ali Jamasb [1] and Seyed-Hani Motavalli-Anbaran [2*]

[1] *Ph.D. Student, Institute of Geophysics, University of Tehran, Iran*
[2] *Associate Professor, Institute of Geophysics, University of Tehran, Iran*

(Received: 20 December 2023, Accepted: 16 March 2024)

Abstract

We present a fast implementation of a 1D elastic full-waveform inversion for reconstructing the elastic structure of the subsurface. The FWI is an inversion algorithm that directly models the full seismic wavefield by solving a semi-analytical form of the elastic wave equation for a 1D layered earth model known as the reflectivity method. The input seismic data are pre-conditioned angle-gathers. The inversion is done using a stochastic algorithm known as PSOES, a fast hybrid stochastic optimization algorithm. Our work primarily contributes to accelerating the computation times required for the inversion, with the goal of developing a strategy that enables code implementation at production scales. Additionally, we are working on creating a framework for conducting joint inversions with potential field data. The computational cost of the FWI is directly proportional to the number of unknowns in the inversion problem, which correlates with the vertical resolution of model (i.e., the layer thicknesses in the 1D Earth model) and the maximum depth of the study. However, the relationship is not linear because increasing the number of unknowns affects the run time of both the forward and inverse problems. On the other hand, the quality of the solution highly depends on the vertical resolution since modeling the higher frequencies in the data requires a relatively small vertical thickness. An optimum implementation of the FWI could result in calculating 1D elastic profiles of the subsurface which could be used for constraining the inversion of potential field data over sedimentary basins.

Keywords: Seismic waveform inversion, stochastic inversion, PSOES, reflectivity method

[*]Corresponding author: motavalli@ut.ac.ir

1 Introduction

Seismic Full-Waveform Inversion (FWI) has received tremendous attention in recent years because of its superior performance in both imaging applications (e.g., Alaei et al., 2022; Gong et al., 2023; McLeman et al., 2023; Warner et al., 2021) as well as elastic formulations with direct quantitative interpretation applications (e.g., Hu et al., 2023; Wang et al., 2021; Martin and Long, 2019; Zhang et al., 2018; Ghanbarnejad Moghanloo et al., 2017; Moghanloo et al., 2018).

In general, FWI is a high-demanding computational approach and the availability of high-performance computing is an integral part of its successful utilization (e.g., Bortot et al., 2023; Tarayoun et al., 2022; He et al., 2018). As an inverse problem, the FWI is highly non-linear (Wu, 2018; Virieux and Operto, 2009) and essentially requires a relatively optimum starting model which has to either come from seismic processing or other inversion schemes such as travel-time tomography (Treister and Haber, 2017; Biondi and Almomin, 2014; Alkhalifah and Choi, 2013). The non-linearity is partly caused by the simultaneous reconstruction of low and high frequency content of the data which are sometimes separated in a multi-stage manner to overcome the non-linearity (e.g., Oh et al., 2020). These limiting factors renders the effective application of FWI quite problematic for standard day-to-day workstations as even the available benchmark data are considered big data (e.g., Deng et al., 2022).

Compared to three- and two-dimensional elastic FWI problems, 1D elastic FWI is particularly more robust for a number of reasons including the possibility to use global stochastic inversion algorithms (e.g., Aguiar et al., 2019). However, the underpinning reason for this is the forward problem which could be solved (semi-) analytically as opposed to numerical solvers and hence faster implementations (Santos and Revelo, 2018). In addition, the location of the inversion could be selected based on prior information which facilitates detailed investigations over selected target areas. The 1D nature also allows easy implementations of greedy parallel computing techniques as well as computationally expensive probabilistic inversion algorithms for uncertainty analysis (e.g., Markov Chain Monte Carlo methods) which are quite advantageous from a practical standpoint (e.g., Aleardi et al., 2016).

From the standpoint of integrated and/or joint inversion of seismic waveform and potential field data, the high cost of 2D/3D FWI is a limiting factor. While several works have recently investigated, for instance, joint FWI and gravity inversion (e.g., Jiang, 2020; Sirtori et al., 2019; Silva et al., 2018), the practical appropriateness of such endeavors are still debatable. In theory, such joining of the two methods would be advantageous in recovering areas with sharp lateral variations in velocity/density especially, in the presence of salt structures, over thrusting, and/or basalts where seismic has difficulties (e.g., Sanford et al., 2023; Hu et al., 2022). However, other than marine seismic surveys, gravity and seismic data are hardly collected together. On the other hand, constraining gravity/magnetic and/or magnetotelluric data with well measurements is quite common (e.g., Lyrio and Li, 2023; Sun et al., 2019; Davis, 2019). To this end, 1D FWI is well suited for constraining potential field data in the form of pseudo wells which is the ultimate goal for the current contribution.

In the following, the problem statement and related definitions of 1D FWI are first presented, followed by the implementation and acceleration of the reflectivity method, as the forward problem. Next, we discuss the formulation of the inversion and present numerical tests

and conclusion.

2 1D elastic Full-Waveform Inversion problem statement

The FWI problem is defined as mathematically finding a set of elastic parameters of the subsurface (compressional and shear wave velocities and density, hereafter model) which can produce a seismic response that matches the observed one. The FWI is a one-dimensional problem meaning that the model is defined as a stack of laterally homogeneous layers. It is also a non-linear problem since there is no linear relationship between the model and seismic data. The model is defined as the vector of subsurface elastic parameters of size $\boldsymbol{M\times 3}$ with $\boldsymbol{M}$ being the number of layers in the model. The FWI is solved here using a global optimization algorithm for optimizing a single-valued objective function (Jamasb et al., 2019). The stochastic algorithm explores a search space defined as a subset of $\Re^M$ with an upper and lower bound, shown here as $\boldsymbol{UB}$ and $\boldsymbol{LB}$, respectively. The fitness of the solution is measured as a single value through defining an objective function:

$$\varphi(\boldsymbol{m}) = \sum_{i=1}^{N} w_i\left[d_i^{obs} - d_i^{cal}\right]^2 + \mu S(\boldsymbol{m}) \quad (1)$$

where the first term on the right-hand side is the fitness of model $\boldsymbol{m}$ in which $\boldsymbol{w_i}$ is an element-wise data weight (e.g., data uncertainty) and $\boldsymbol{N}$ is the total number of the observed data. $\boldsymbol{S(m)}$ is a stabilizing operator and $\boldsymbol{\mu}$ is the stabilizing parameter. One example of $\boldsymbol{S(m)}$ is the smoothing functional (i.e., the norm of the first derivative of the model parameters) which ensures that the estimated model not only has an acceptable misfit but also has minimum roughness aiming to suppress any artifacts in the estimated model. The FWI problem is mathematically defined as finding the optimal $\boldsymbol{m^{optimal}}$ as:

$$find\ \boldsymbol{m} = \boldsymbol{m^{optimal}}\ if\ \ \varphi(\boldsymbol{m}) \leq \varphi\left(\boldsymbol{m^k}\right)\ \forall\ \boldsymbol{m^k} \in [\boldsymbol{LB}, \boldsymbol{UB}] \quad (2)$$

where $\varphi(\boldsymbol{m})$ is the objective function.

3 1D elastic FWI forward problem: The reflectivity method

The FWI problem solves a semi-analytical form of the wave equation using the reflectivity method [e.g., Mallick (1999)], first developed by Fuchs (1968) and Fuchs and Müller (1971). The reflectivity method was later improved by Kennett (1975), Kind (1977), Kennett and Kerry (1979), and Fryer (1980). This method uses the response of stack of horizontal elastic layers to an incident harmonic wave of frequency ω and angle of incidence θ which can be computed by the well-known Thompson-Haskell matrix formalism (Haskell, 1953) in terms of the reflection and transmission properties of portions of the stratification. In the original reflectivity method (Fuchs and Müller, 1971), the reflective response of a stack of layers was calculated by performing the inverse spatial transform as an integral over real angles of incidence. The method was later generalized to include the complete response (P-P reflections, P-S conversions, and multiples) of a multi-layered heterogeneous medium with, for instance, the free surface (Müller, 1985).

The reflectivity method uses the reflection and transmission coefficients (or reflectivities and transmissivities) for plane waves incident on a plane interface or a stack of homogeneous layers separating two homogeneous half-spaces. The coefficients for an interface are given analytically by Müller (1985) which we do not repeat here. However, those for a stack of layers are derived by a recursive algorithm first described by Kennett (1974) and in more details by Kennett (2009). To our knowledge, the partial reflection coefficients, although previously derived theoretically, have not been used in seismic exploration workflows.

In order to calculate the overall reflec-

tion coefficients for a simple two-layers (AB and BC) model, let R_D^{AB} represent the reflection coefficients of a down-going (hence subscript D) P-wave reflected from the interface separating A and B layers (Fig. 1). Similarly, T and U are used for transmission and up-going incident waves, respectively. The aim of the recursive scheme is the calculation of R_D^{AC}, i.e., the overall reflection response of the two-layers model (Kennett, 2009):

$$R_D^{AC} = R_D^{AB} + T_U^{AB} R_D^{BC} [I - R_U^{AB} R_D^{BC}]^{-1} T_D^{AB} \quad (3)$$

where the $[I - R_U^{AB} R_D^{BC}]^{-1}$ term in Eq. (3) can be decomposed as:

$$[I - R_U^{AB} R_D^{BC}]^{-1} = I + R_U^{AB} R_D^{BC} + R_U^{AB} R_D^{BC} R_U^{AB} R_D^{BC} \quad (4)$$

From which, $(10 R_D^{AC} = R_D^{AB} + T_U^{AB} R_D^{BC} [I - R_U^{AB} R_D^{BC}]^{-1} T_D^{AB})$ becomes:

$$R_D^{AC} = R_D^{AB} + T_U^{AB} R_D^{BC} T_D^{AB} + T_U^{AB} R_D^{BC} R_U^{AB} R_D^{BC} T_D^{AB} + \cdots \quad (5)$$

The sequence in Eq. (5) is illustrated schematically in Figure 1 where we have envisaged some incident downward travelling wave at z_A giving rise to both reflection and transmission terms. The physical content of each of the terms in Eq. (5) can be found by reading it from **right** to **left**.

For the reflection series, R_D^{AB} is just the reflection matrix for the region 'AB' in isolation. The second term $T_U^{AB} R_D^{BC} T_D^{AB}$ represents waves which have been transmitted through the upper region and then been reflected by the region 'BC' and finally, transmitted back through the upper zone. In $T_U^{AB} R_D^{BC} R_U^{AB} R_D^{BC} T_D^{AB}$, we have the same set of interactions as in the previous term but in addition, we include waves reflected down from the upper region to z_B and then reflected back from the region 'BC' before passage to z_A. The higher terms in the series include further internal interactions between the zones 'AB' and 'BC'.

The generic geometry of the problem is shown in Figure 2. The structure consists of a water layer of depth h and uniform sound velocity α_0. The reflection zone begins at the ocean bottom and includes all deeper structures. We consider a receiver at a depth z from the surface and a horizontal distance r from an explosive source with a displacement potential time function s(t). The displacement potential is calculated using the Fourier transform, with variables including the reflection coefficient at the ocean bottom, horizontal and vertical wavenumbers, and a reflectivity function that could account for multiple reflections and wave interconversions. The vertical displacement is derived from the displacement potential by taking the derivative with respect to depth. A substitution is made to express the equation in terms of slowness, leading

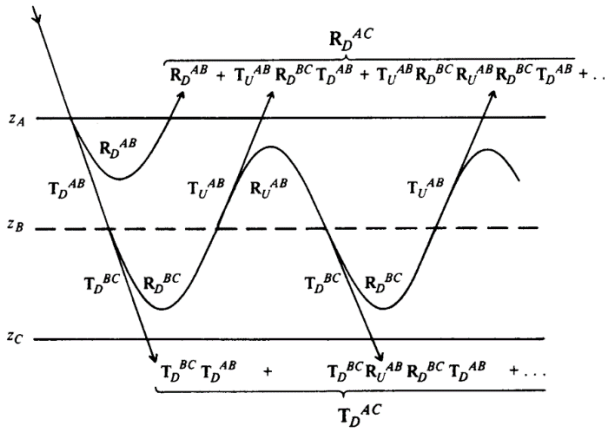

Figure 1. Schematic representation of the first few terms in the reflectivity series calculation (Kennett, 2009).

For the calculation of the displacement potentials due to a single source, we rely on the derivation of Fryer (1980).

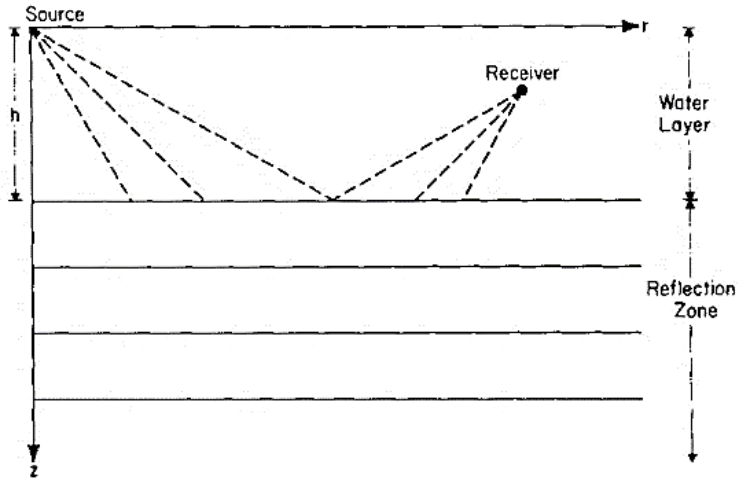

Figure 2. The response of a layered half-space (the reflection zone) to a point source at the surface of an overlying water layer is to be synthesized. Direct and surface reflected phases are ignored (Fryer, 1980).

to the slowness integral. The horizontal slowness and vertical slowness are defined, and the time function is obtained as the inverse Fourier transform of the slowness integral.

In the original reflectivity method, the slowness integral is evaluated numerically for each frequency at a desired range *r*. This results in a frequency series which is inverse Fourier transformed to give a time series which when convolved with an appropriate source function yields the desired synthetic traces. Therefore, the calculation of the synthetic traces in the time domains requires:

1. *Calculation of the total reflection coefficient for the reflection zone;*
2. *Calculation of the inverse Hankel transform;*
3. *Calculation of the inverse Fourier transform.*

Assuming non-dissipative media, the velocities are not dependent on frequency meaning that the reflectivities which are functions of velocity are also independent of frequency and can be calculated once for each value of slowness. If the order of the two transforms is interchanged, intermediate results are time series for particular values of slowness. This is particularly of interest because the slowness can then be transformed to the angle of incidence θ using the equation $\theta = \sin^{-1}(p\alpha_0)$. In other words, if the FWI calculations are done in the angle domain (i.e., the data are transformed into angle domain using a slant-stack), the calculation of the inverse Hankel transform as well as its corresponding Bessel functions are not needed. As a result, the forward problem simplifies to the following equation (Fryer, 1980):

$$w(\theta, z, t) = -\frac{1}{2\pi}\, s(t) * \int_{-\infty}^{+\infty} R_{pp}(\omega, \theta) e^{j\omega t} d\omega \qquad (6)$$

where $*$ indicates convolution in the time domain.

4 Stochastic inversion (PSOES)

A stochastic non-linear geophysical inversion can be described as the process of finding the global solution, that is, the solution that has outperformed the others in terms of minimization of the cost function. These methods offer simplicity in constructing a cost function that best suits the needs of the problem. A general cost function can be defined as (Jamasb et al., 2021):

$$\varphi(\boldsymbol{m}) = \sum_{i=1}^{N} w_i \left[d_i^{obs} - d_i^{cal}\right]^p + \mu S(\boldsymbol{m}) + \sum_{j=1}^{M} (\lambda_j \left| m_j - m_j^{apr} \right|) \qquad (7)$$

where the first term on the right-hand side of Eq. (7) is the data misfit in which w_i is an element-wise data weight (e.g., data uncertainty), N is the total number of the observed data and p indicates the norm of the misfit calculation. $\boldsymbol{m}$ is the

vector of model parameters, $d_i^{cal} = f(\boldsymbol{m})$ is the calculated data and $S(\boldsymbol{m})$ is a stabilizing operator. The last term is for explicit *a priori* information, in which λ_j is nonzero for points where explicit a priori information m^{apr} is used.

Global stochastic optimization algorithms carry out their search by means of two different approaches that are based on the concepts of exploration and exploitation of the search space. The former is concerned with finding the neighborhood of the global minimum/maximum while the latter tries to improve the approximation of the global solution within that neighborhood towards the true global minimum. The optimization process is performed iteratively by simultaneously probing several independent potential solutions at each iteration. The cost function is calculated for each potential solution to assess its fitness. The required computational resources for a successfully converging inversion thus directly depend on the calculation of the forward problem which has to be calculated at least a total of $\boldsymbol{N_{pop}} \times \boldsymbol{N_{iter}}$ times during the inversion. However, difficulty arises in setting the aforementioned parameters since they are problem-related. Complexity as well as non-linearity of the cost function and the number of model parameters (i.e., the dimension of model space) have the strongest influence on setting the values of $\boldsymbol{N_{pop}}$ and $\boldsymbol{N_{iter}}$.

Setting optimum numbers of iterations and initial solutions assures that the global solution is selected only after the search space has been efficiently probed in its entirety, and also the approximated global solution is in fact as close as it can be to the true global minimum of the cost function. A general workflow for a stochastic inversion includes:

- *Defining the cost function;*
- *Defining the model space in terms of its dimensions and upper and lower bounds in which the search will take place;*
- *Performing the search.*

where the inversion is usually repeated for several sets of pre-set parameters to measure the variability of the stochastic inversion algorithm due to the random initial solution and random paths taken in the search-space throughout the search. In addition to the aforementioned parameters, each stochastic algorithm has a set of native parameters which control its performance in terms of creating a balance between exploration and exploitation stages of the search. In this work, the inversion is carried out using a stochastic global optimization algorithm called PSOES (Jamasb et al., 2019), a hybrid of Particle Swarm Optimization (PSO) and Evolution Strategy (ES) which solves single-objective real-valued continuous optimization problems.

The PSOES is the product of hybridization of PSO and ES. It has been shown in the literature that introducing a discrete behavior into the PSO algorithm results in superior performance of the algorithm in terms of how much computational time per model parameter is required for a successful run. The details of the stochastic algorithm used can be found in Jamasb et al. (2019) and Jamasb et al. (2021).

5 Numerical implementation of the forward problem

The stochastic inversion is an iterative process. In each iteration, the algorithm performs a set of forward calculations from a set of randomly generated candidate solutions and selects the best ones to lead the search for the next iteration. Both the number of random candidate solutions, $\boldsymbol{N_{pop}}$, and maximum number of iterations, $\boldsymbol{N_{iter}}$, are user-given parameters. Other than the forward, the rest of the algorithm components are basic mathematical calculations which are inherently simple, and thus fast. As a result, the forward algorithm is the main deciding factor in the run-time of the FWI as the time required for intermediary calcu-

lations is essentially negligible. The run time of a single FWI (i.e., T_{FWI}) is mostly dependent on the time that the forward problem takes ($T_{FWI} = \boldsymbol{N_{pop}} \times \boldsymbol{N_{iter}} \times T_{forward}$). It should be noted that while the inversion time is linearly dependent on the forward time, the latter itself varies non-linearly by addition of layers. There is also an overhead time required for I/O handling. Based on synthetic tests, for a model with 250 layers (i.e., 3×250=750 unknowns) at least 25000 forward calculations are required (e.g., $\boldsymbol{N_{pop}}$=100 and $\boldsymbol{N_{iter}}$=250) to achieve a meaningful solution. Thus, the run-time of the forward calculation is the most important factor in the successful implementation of the FWI.

Table 1. PSOES algorithm (Jamasb et al., 2019).

Set the population size (Npop) and maximum iterations (Niter)
Set the mutation pressure (p) and mutation constant c
Set the boundaries of the search-space
Randomly initialize particle positions within the bounds of search space
Evaluate fitness values for the population using the cost function
Update **global best position*** (gbest)
Set the initial positions as the vector of personal best positions
Loop over iterations (1→Niter)
◦ Loop over particles (1→Npop)
◦ ◦ Update the velocities
◦ ◦ Update the positions
◦ ◦ Evaluate the fitness of particles
◦ ◦ Draw a random number r
◦ ◦ if r<p (mutation pressure)
◦ ◦ ◦ Mutate the positions
◦ ◦ ◦ Evaluate the fitness and select the fittest solution
◦ ◦ Update the personal bests
◦ ◦ Update the **global bests**
◦ End loop over particles
End loop over iterations

*The output of the inversion algorithm (Global Best Solution, gbest)

There are three loops in the calculation of $R_{pp}(\omega, p)$, outermost loops of p, middle loops of layer n, and innermost loops of ω. Generally, slowness is fixed at each outermost loop, and the angle of incidence changes over each layer, i.e., $\theta_n = \arcsin(\alpha_n p)$. But we set the angle of incidence to be fixed at each outermost loop; thus, slowness changes over each layer. Therefore, $R_{pp}(\omega, p)$ is resampled as $R_{pp}(\omega, \theta)$, and the outcome is actually an angle gather. Additionally, we removed the loop on frequency through a vectorization scheme which allows for parallel calculation of all frequencies at once. Our algorithms follow the algorithms from Müller (1985) for the calculation of R_{pp}. We also considered the works by Mallick (1999), Fryer (1980) and Kennett (2009) for optimizing the computer implementation of our algorithm.

In order to avoid time aliasing, the frequency integrand in the forward algorithm$\varphi(\boldsymbol{m}) = \ i = 1⍰N⍰w_i\left[d_i^{obs} - d_i^{cal}\right]^p + \mu S(\boldsymbol{m}) + \ j = 1⍰M⍰(\lambda_j m_j - m_j^{apr}⍰)⍰⍰$ must be adequately sampled in ω. To prevent aliasing without increasing the computational burden, the concept of complex frequencies (Mallick and Frazer, 1987) is used which allows attenuating the energy that is wrapped around from times greater than T (the length of seismogram) by $e^{-\tau t}$. Our reflectivity algorithm takes τ (tau) as input. The synthetic tests as well as real tests showed that a range of 10 to 200 is optimum for setting tau. Setting tau is especially important when the given length for the synthetic trace is smaller

than the true earth response. The effect of tau is demonstrated in Figure 3.

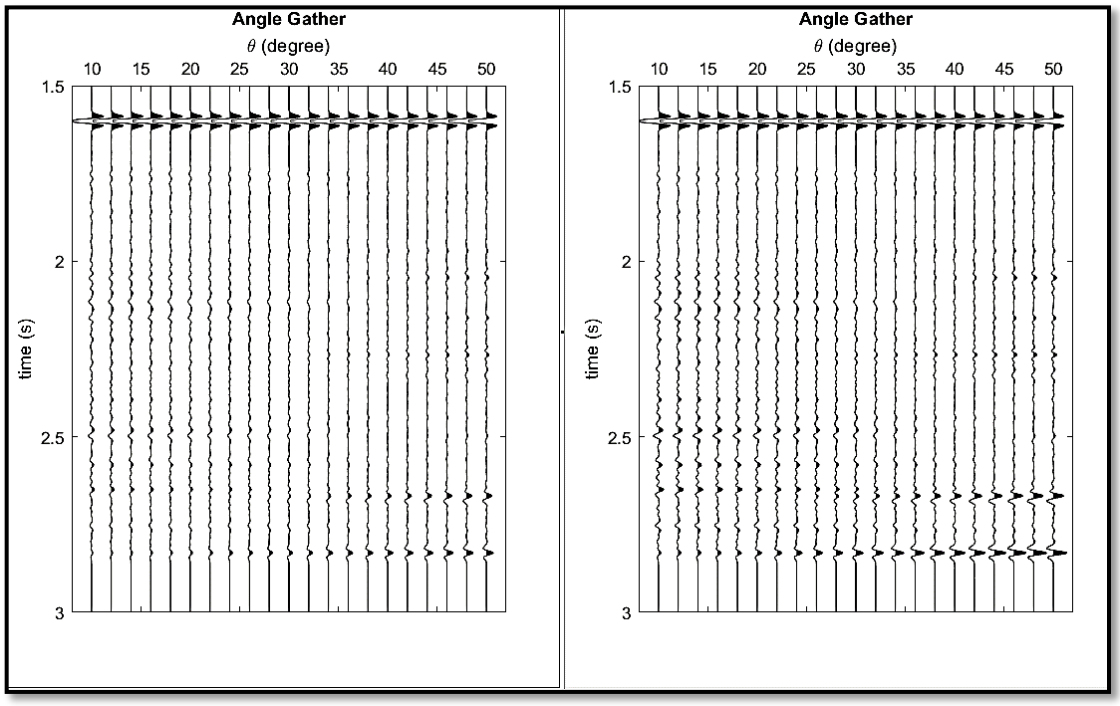

(a) (b)

Figure 3. The use of complex frequencies. (a) tau=15. (b) tau=100.

The developed forward algorithm is capable to generate synthetic seismograms with or without NMO correction through a change in the phase matrix. It is also capable to generate full seismic response or partial response in terms of converted waves and multiples. These variations are shown in Figure 5 to 7 for the model presented in Figure 4.

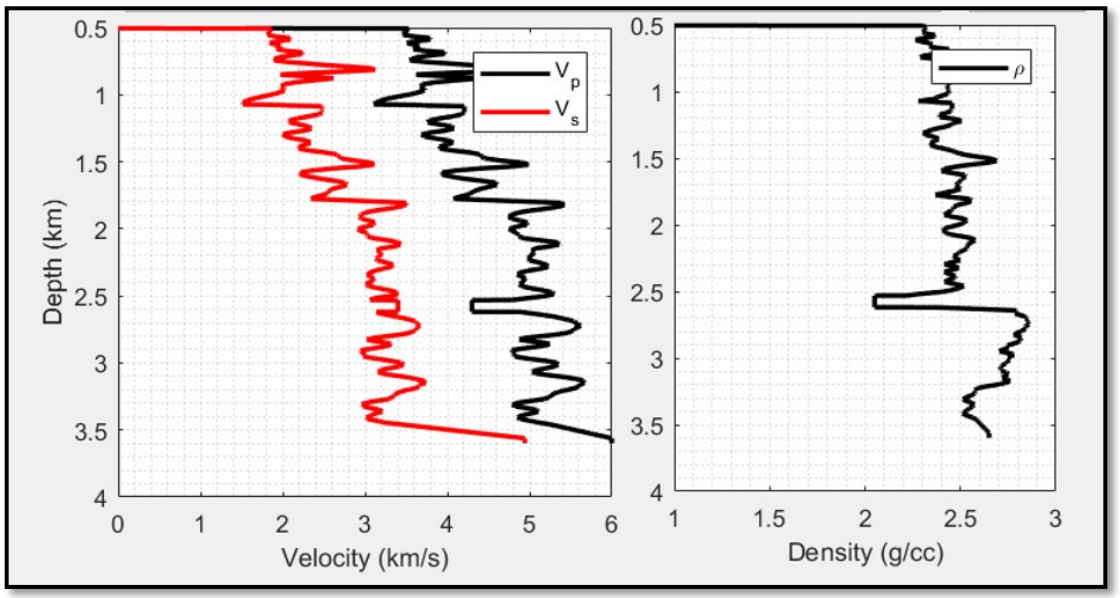

Figure 4. The synthetic model.

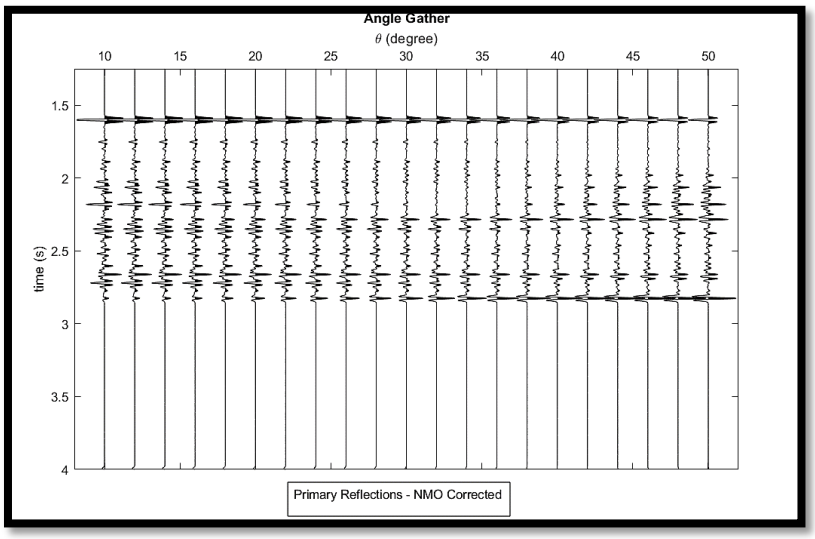

Figure 5. Results of the forward algorithm: NMO-Corrected primaries.

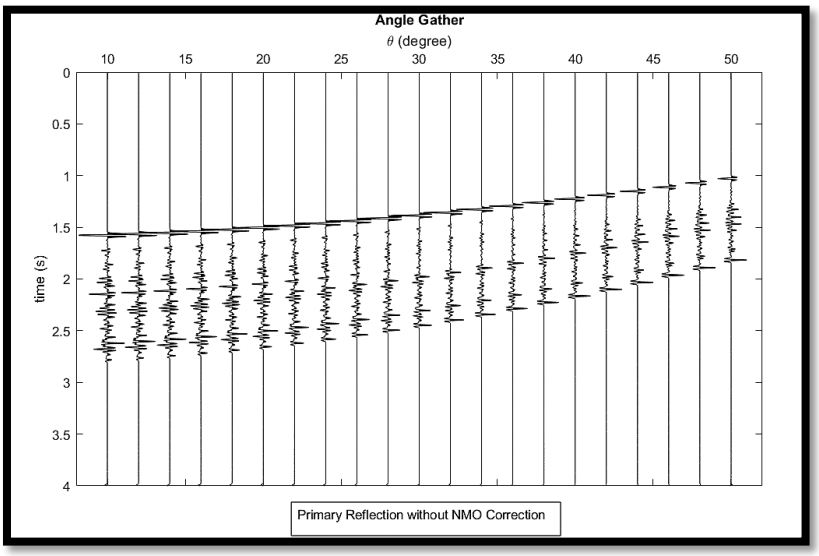

Figure 6. Results of the forward algorithm: Primaries.

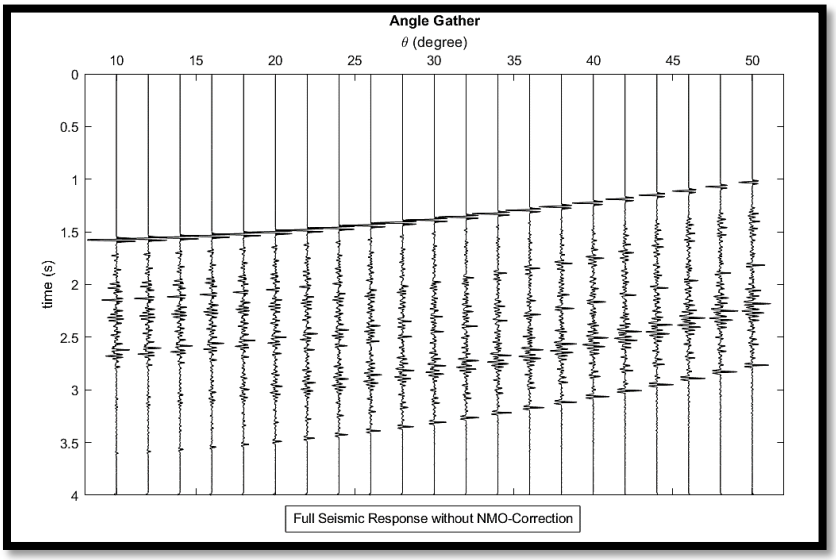

Figure 7. Results of the forward algorithm: Full seismic response.

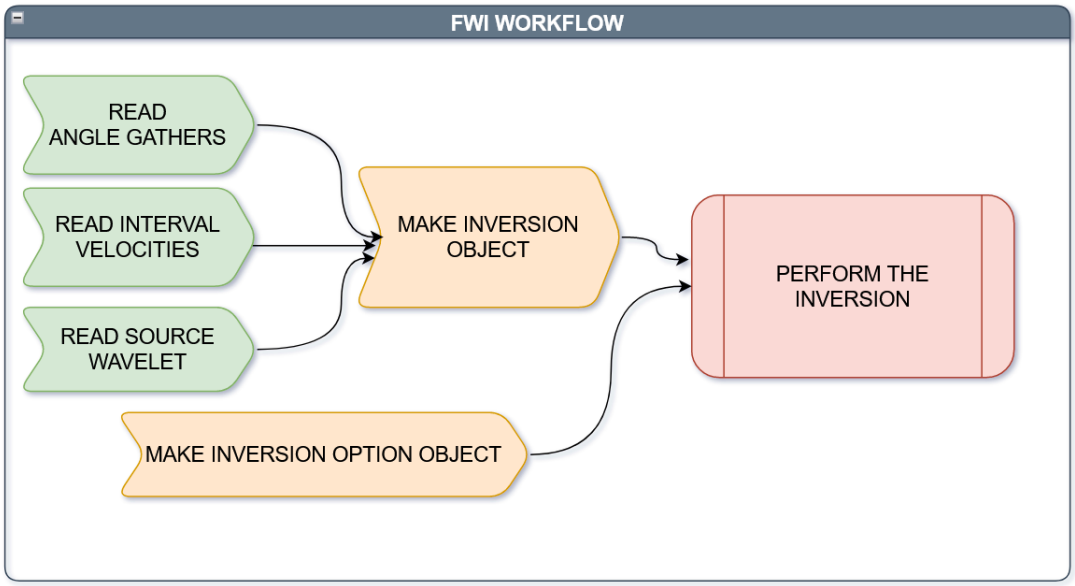

Figure 8. The FWI workflow. The items in green refer to input data reading. The orange items require user–sets parameters.

Table 2. Synthetic inversion parameters.

Name	Value
Frequency Range	**[0-80] Hz**
Layer Thickness	**60 m**
Number of Layers	**37**
Total time	**3 s (df=0.4 Hz)**
Dt	**0.002 s**
NMO correction	**True**
Angle range	**[2-30]**

6 Numerical tests on inversion

The overall workflow for the FWI is depicted in Fig. 8.

The Mobil-Well logs were used as the model acquired from SEG website as a standard dataset for seismic inversion tests which come from the North Viking Graben in the North Sea. Mobil-Well log data were down-sampled and used for making the synthetic model via the forward algorithm. The forward and inverse parameters are given in Table *2*.

The results of the inversion using the full seismic wavefield (including multiples and non-NMO corrected) are presented in Figure 9. Using the full seismic wavefield has allowed the algorithm to fully recover the synthetic model. The data fits are shown in Figure 10.

7 Discussion on numerical tests

An important practicality in using the FWI is the available data. In this work, we focused on a marine situation where the 1D assumption is more reasonable than in onshore. In theory, the best approach is to use non-NMO corrected input seismic data with multiples which allows the inversion to better constrain the sharp changes as well as long-wavelength structures. In case that the data are NMO-corrected and without multiples, the performance of the algorithm drops. In the following, an inversion test on only primary waves without multiples is presented (Figure 11 and 12). While the inversion has been successful in recovering the low velocity zone at the depth of 2 km, the quality of the fit between the true model and the recovered

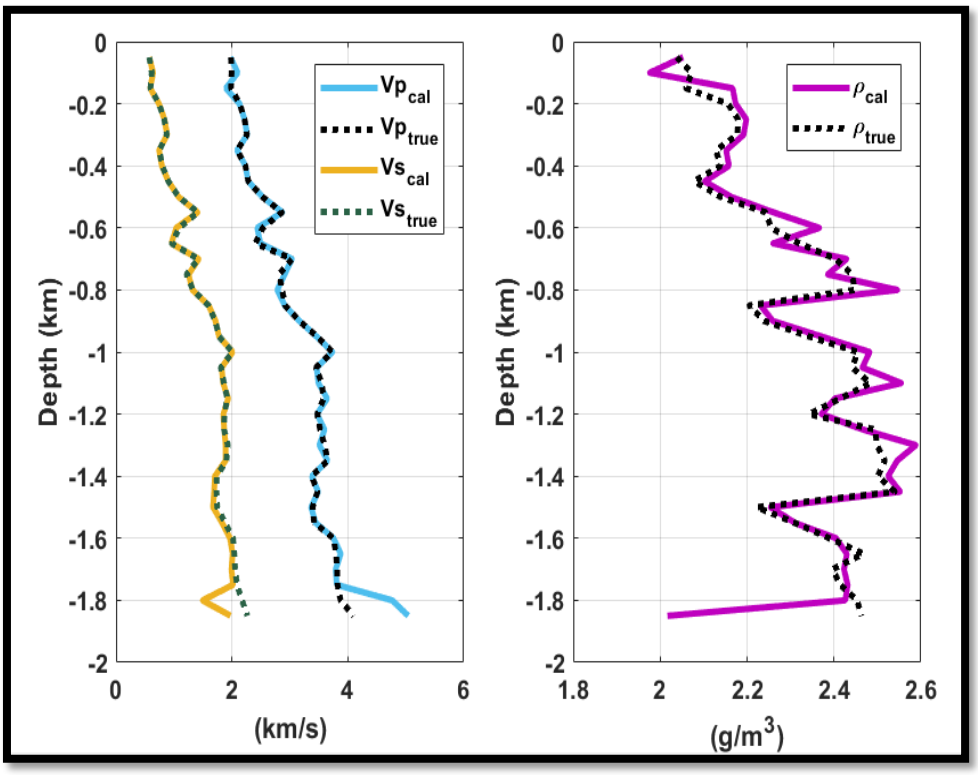

Figure 9. Results of the test inversion - Recovered model.

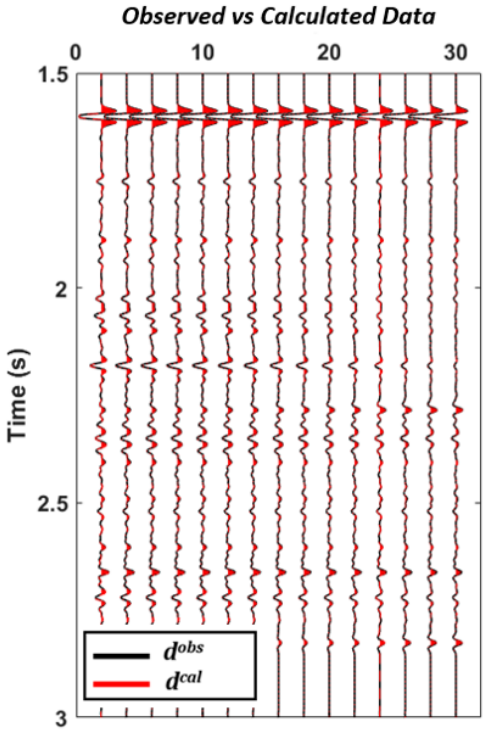

Figure 10. The final data fit for the recovered model of Figure 9.

one is not as high as in the previous case. The main difference between the two inversions is the seismic response used. In the previous inversion, the full seismic response including multiples and converted waves was given as input to the inversion. While usually multiples are considered as liability, which could result

in false interpretation, for the inversion they provide valuable added information which can be used to better constrain the model. Also, the converted waves are excellent for the recovery of sharp structures and also the shear wave structure.

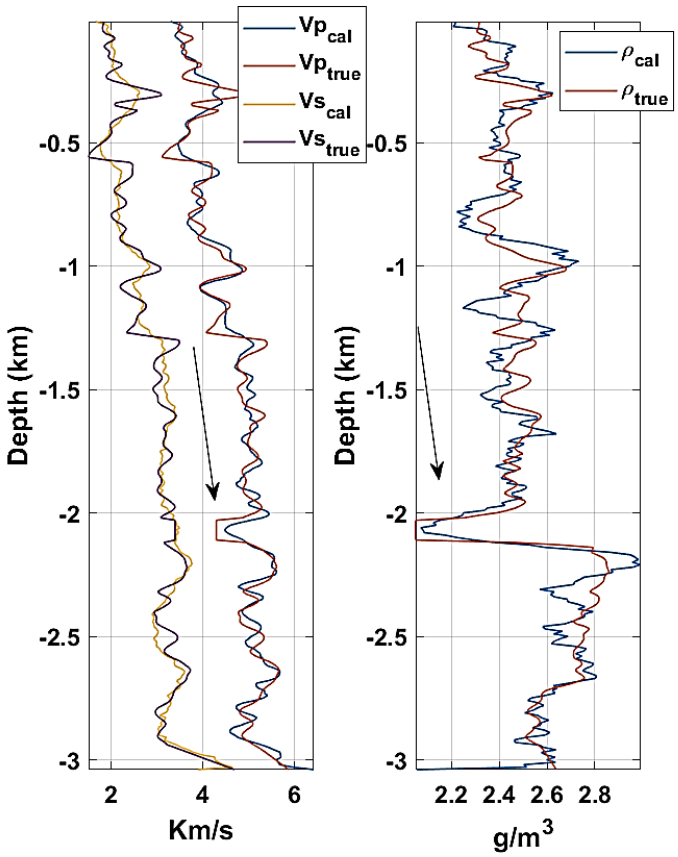

Figure 11. The result of NMO-corrected primary reflections without multiples. The recovered low-velocity zones are shown by black arrows.

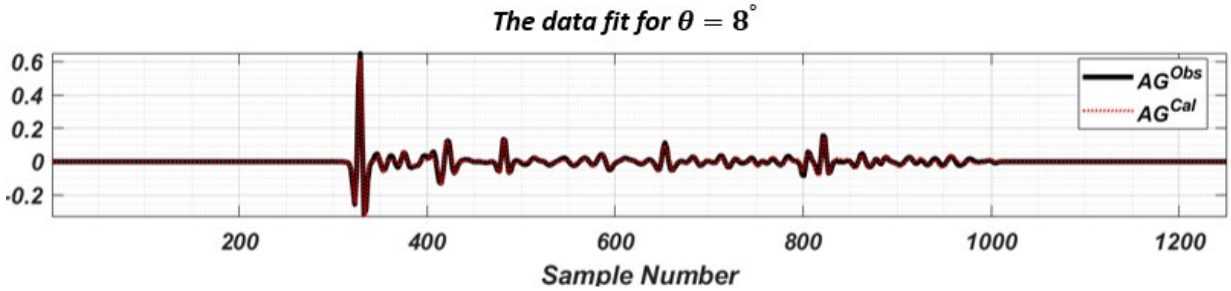

Figure 12. A sample of data fit for the results in Figure 11.

Additionally, there are arguments in the literature [e.g., Mallick (1999)] for using non-NMO corrected data because they can provide valuable long-wavelength information for the inversion. Lastly, the tests showed that using primary reflections as input data is more effective in recovering the compressional velocity and density than the shear velocity.

Another important issue is the vertical resolution of the model. In order to be able to fit high frequency content of the data, the layer thicknesses should be accordingly small. However, that would complicate the inversion in two different ways. First, because the forward algorithm has a loop over the number of layers, a too small layer thickness means greater calculation time for each forward. Secondly, and arguably more important-

ly, increasing the number of layers means increasing the number of unknowns that the inversion has to recover. It is well known that the number of solution candidates in any stochastic inversion algorithm directly depends on the size of model space [i.e., 3×number of layers, e.g., Jamasb et al. (2019)]. This means that by decreasing the layer thickness, the inversion is forced to calculate more forward algorithms in each iteration which itself is more time costly. As a result, the relationship between the vertical resolution and the calculation burden is not linear, meaning that decreasing the layer thickness by a factor of 2 (half the original thickness) does not necessarily mean twice the calculation.

An important subject in an inversion is the uncertainty of the model. In principle, since stochastic inversion algorithms work with random numbers, several runs of the algorithm could and usually do result in slightly different solutions. Therefore, a first order uncertainty analysis is possible simply by repeating the inversion. With each solution considered as a random variable, any statistical criterion (e.g., standard deviation) could be used to measure the uncertainty of the solution (Jamasb et al., 2021). However, setting the number of required repeated inversions is not actually straightforward. In practice, the number of repeated inversions must be large enough so that distribution of the random solutions at each calculation point becomes stationary.

8 Conclusion

We presented the conceptual framework as well as numerical tests on a 1D seismic full-waveform inversion (FWI) algorithm. FWI is a powerful imaging tool, capable of generating subsurface models that depict seismic velocities and density at a fine resolution. It is particularly valuable for near-surface applications, where depth penetration ranges from tens to hundreds of meters, as it does not require the separation of different seismic phases such as direct waves, reflections, and surface waves. Furthermore, FWI can be utilized to obtain high-resolution multi-parameter images. The forward problem is based on the reflectivity method, a semi-analytical method to solve the wave equation which is capable of generating the full seismic field. For the inversion, we used the PSOES algorithm, a global search method developed for non-linear geophysical inversions. We tested our method by using both the full seismic wavefield and also on only primary reflections. Overall, using only NMO-corrected primary reflections as input as opposed to the full seismic response of the Earth results in a relatively fast inversion since the latter takes more time to calculate, and the input preparation is also not costly. However, the downfall is the loss of sharp structures in the recovered model and also less constraining of the shear velocity structure.

References

Aguiar, R., Neto, A., Bezerra, Y., Henriques, M., Nascimento, H., and Lucena, L., 2019, A global optimization DFO-CRS strategy for 1D Full Waveform Inversion: Journal of Computational Interdisciplinary Sciences, **10**(1), 21-30.

Alaei, N., Soleimani Monfared, M., Roshandel Kahoo, A., and Bohlen, T., 2022, Seismic imaging of complex velocity structures by 2D pseudo-viscoelastic time-domain full-waveform inversion: Applied Sciences, **12**(15), 7741.

Aleardi, M., Tognarelli, A., and Mazzotti, A., 2016, Characterisation of shallow marine sediments using high-resolution velocity analysis and genetic-algorithm-driven 1D elastic full-waveform inversion: Near Surface Geophysics, **14**(5), 449-460.

Alkhalifah, T., and Choi, Y., 2013, From tomography to FWI with a single

objective function: 75th EAGE Conference & Exhibition incorporating SPE EUROPEC 2013.

Biondi, B., and Almomin, A., 2014, Efficient and robust waveform-inversion workflow: Tomographic FWI followed by FWI: SEG Technical Program Expanded Abstracts 2014 (pp. 917-921), Society of Exploration Geophysicists.

Bortot, L., Bienati, N., and Panizzardi, J., 2023, HPC Implementation of the FWI Gradient Reduction Stage: EAGE Seventh High Performance Computing Workshop.

Davis, K., 2019, Application of growing-body potential-field inversion from drillholes: ASEG Extended Abstracts, **2019**(1), 1-4.

Deng, C., Feng, S., Wang, H., et al., 2022, OpenFWI: large-scale multi-structural benchmark datasets for Full Waveform Inversion: Advances in Neural Information Processing Systems, **35**, 6007-6020.

Fryer, G. J., 1980, A slowness approach to the reflectivity method of seismogram synthesis: Geophysical Journal International, **63**(3), 747-758.

Fuchs, K., 1968, The reflection of spherical waves from transition zones with arbitrary depth-dependent elastic moduli and density: Journal of Physics of the Earth**, 16**(Special), 27-41.

Fuchs, K., and Müller, G., 1971, Computation of synthetic seismograms with the reflectivity method and comparison with observations: Geophysical Journal International, **23**(4), 417-433.

Ghanbarnejad Moghanloo, H., Riahi, M. A., Bagheri, M., and Seyedali, S. M., 2017, Determining the area of reser-voir using simultaneous inversion of seismic data: Iranian Journal of Geo-physics, **11**(3), 45-56.

Gong, B., Li, T., Lee, K. S., Meng, Z., Zhang, K., Bibolova, A., and Katrenov, Z., 2023, Application of Q-FWI-tomography and least-squares migration to improve seismic resolution in Tengiz oil field: The Leading Edge, **42**(3), 156-164.

Haskell, N., 1953, The dispersion of surface waves in multi-layered media: Bulletin of the Seismological Society of America, **43**, 17-43.

He, Y., Liu, L., and Luo, Y., 2018, A practical implementation of 3D full-waveform inversion on heterogeneous HPC systems: International Geophysical Conference, Beijing, China, 24-27 April 2018.

Hu, Q., Eaid, M., Keating, S., Innanen, K., and Cai, X., 2023, Quantitative FWI characterization of reservoir properties at the CMC Newell County Facility: SEG International Exposition and Annual Meeting.

Hu, Y., Fu, L.-Y., Deng, W., Li, Q., and Huang, X., 2022, Joint traditional and reflection envelope inversion: IEEE Geoscience and Remote Sensing Letters, **19**, 1-5.

Jamasb, A., Motavalli-Anbaran, S.-H., Entezar-Saadat, V., and Zeyen, H., 2021, Multiscale nonlinear inversion of gravity data for depth-to-basement estimation via coupled stochastic-deterministic optimization: Geophysics, **86**(6), G99-G112.

Jamasb, A., Motavalli-Anbaran, S.-H., and Ghasemi, K., 2019, A novel hybrid algorithm of particle swarm optimization and evolution strategies for geophysical non-linear inverse problems: Pure and Applied Geophysics, **176**, 1601-1613.

Jiang, W., 2020, 3-D joint inversion of seismic waveform and airborne gravity gradiometry data: Geophysical Journal International, **223**(2), 746-764.

Kennett, B., 1974, Reflections, rays, and reverberations: Bulletin of the Seismological Society of America, **64**(6), 1685-1696.

Kennett, B., 1975, The effects of attenuation on seismograms: Bulletin

of the Seismological Society of America, **65**(6), 1643-1651.

Kennett, B., 2009, Seismic Wave Propagation in Stratified Media: ANU Press.

Kennett, B., and Kerry, N., 1979, Seismic waves in a stratified half space: Geophysical Journal International, **57**(3), 557-583.

Kind, R., 1977, The reflectivity method for a buried source: Journal of Geophysics, **44**(1), 603-612.

Lyrio, J. C. S., and Li, Y., 2023, Basement mapping using nonlinear gravity inversion with borehole and seismic constraints: Minerals, **1**3(9), 1173.

Mallick, S., 1999, Some practical aspects of prestack waveform inversion using a genetic algorithm; an example from the East Texas Woodbine gas sand: Geophysics, **64**(2), 326-336.

Mallick, S., and Frazer, L. N., 1987, Practical aspects of reflectivity modeling: Geophysics, **52**(10), 1355-1364.

Martin, T., and Long, A., 2019, The evolution of FWI and its perceived benefits: The APPEA Journal, **59**(1), 432-443.

McLeman, J., Rayment, T., Burgess, T., Dancer, K., Hampson, G., and Pauli, A., 2023, Superior resolution through multiparameter FWI imaging: A new philosophy in seismic processing and imaging: The Leading Edge, **42**(1), 34-43.

Moghanloo, H. G., Riahi, M. A., and Bagheri, M., 2018, Application of simultaneous prestack inversion in reservoir facies identification: Journal of Geophysics and Engineering, **15**(4), 1376-1388.

Müller, G., 1985, The reflectivity method: a tutorial: Journal of Geophysics, **58**(1), 153-174.

Oh, J.-W., Shin, Y., Alkhalifah, T., and Min, D.-J., 2020, Multistage elastic full-waveform inversion for tilted transverse isotropic media: Geophysical Journal International, **223**(1), 57-76.

Sanford, O., Hobbs, R., Brown, R., and Schofield, N., 2023, Uncertainties in ray-tracing tomography models used for sub-basalt seismic imaging: Pure and Applied Geophysics, **180**(1), 145-156.

Santos, R. D. S., and Revelo, D. E., 2018, 1D FWI using GA and PSO: unidimensional full waveform inversion with a non-conventional approach of nondeterministic: Rio Oil & Gas Expo and Conference 2018, Rio de Janeiro/Brasil.

Silva, R., De Basabe, J., Sen, M., González-Escobar, M., and Gomez-Treviño, E., 2018, Joint acoustic full waveform and gravimetric inversion*:* SEG International Exposition and Annual Meeting.

Sirtori, A., Mantovani, M., Epifani, A., and Miotti, F., 2019, Integrated simultaneous joint and full-waveform inversion workflow for multiphysics near-surface modeling*:* 81st EAGE Conference and Exhibition 2019.

Sun, S., Chen, C., and Liu, Y., 2019, Constrained 3D inversion of magnetic data with structural orientation and borehole lithology: A case study in the Macheng iron deposit, Hebei, China: Geophysics, **84**(2), B121-B133.

Tarayoun, A., Brossier, R., Cao, J., Jauré, S., Laforêt, S., and Métivier, L., 2022, HPC implementations on SEM46: A 3D modeling and inversion code for anisotropic visco-elastic coupled acoustic media: Sixth EAGE High Performance Computing Workshop.

Treister, E., and Haber, E., 2017, Full waveform inversion guided by travel time tomography: SIAM Journal on Scientific Computing, **39**(5), S587-S609.

Virieux, J., and Operto, S., 2009, An overview of full-waveform inversion in exploration geophysics:

Geophysics, **74**(6), WCC1-WCC26.

Wang, H., Burtz, O., Routh, P., Wang, D., Violet, J., Lu, R., and Lazaratos, S., 2021, Anisotropic 3D elastic full-wavefield inversion to directly estimate elastic properties and its role in interpretation: The Leading Edge, **40**(4), 277-286.

Warner, M., Kalinicheva, T., Mancini, F., and Debens, H., 2021, Keynote: From acquisition to final PSDM volume in days via full-bandwidth FWI: First EAGE Workshop on Optimizing Project Turnaround Performance.

Wu, R.-S., 2018, Untangle the nonlinearity in strong-nonlinear FWI: De-scattering, renormalization and deinterference: International Geophysical Conference, Beijing, China, 24-27 April 2018.

Zhang, Z.-D., Alkhalifah, T., Naeini, E. Z., and Sun, B., 2018, Multiparameter elastic full waveform inversion with facies-based constraints: Geophysical Journal International, **213**(3), 2112-2127.